Robotics and Autonomous Systems 60 (2012) 154–166

Contents lists available at SciVerse ScienceDirect

Robotics and Autonomous Systems

journal homepage: www.elsevier.com/locate/robot

A hierarchical multiple-model approach for detection and isolation of robotic actuator faults

Tesheng Hsiao *, Mao-Chiao Weng

Department of Electrical Engineering, National Chiao Tung University, 1001 Ta Hsueh Rd., Hsinchu, Taiwan

ARTICLE INFO

Article history:
Received 28 October 2010
Received in revised form
10 August 2011
Accepted 14 October 2011
Available online 25 October 2011

Keywords:
Fault detection
Fault isolation
Actuator faults
Robot manipulator
Multiple model
Unscented Kalman filter
GPB-2 algorithm

ABSTRACT

Modern robotic systems perform elaborate tasks in complicated environments and have close interactions with humans. Therefore fault detection and isolation (FDI) schemes must be carefully designed and implemented on robotic systems in order to guarantee safe and reliable operations. In this paper, we propose a hierarchical multiple-model FDI (HMM-FDI) scheme to detect and isolate actuator faults of robot manipulators. The proposed algorithm performs FDI in stages and refines the associated *model set* at each stage. Consequently only a small number of models are required to detect and isolate various types of *unexpected* actuator faults, including abrupt faults, incipient faults, and simultaneous faults. In addition, the computational load is alleviated due to the reduced-sized model set. The relation between the fault detection stage of the HMM-FDI scheme and the likelihood ratio test is explicitly revealed and theoretical upper bounds of the false alarm and missed detection probabilities are evaluated. Then we conduct experiments to demonstrate the ability of the HMM-FDI scheme in successful and immediate detection and isolation of actuator faults.

1. Introduction

Robotic systems are widely used to carry out various missions that require high precision, reliability and safety. Typical robotic applications are, to name but a few, industrial manufacturing, demining, hazardous waste cleanup, and outer space exploration. In addition, recent advances in intelligent robots have inspired a large number of emerging applications such as housekeeping, medical surgeries, and the elderly home care. In order to accomplish these increasingly elaborate tasks, modern robots turn into ever complicating systems. However, the more complex the robotic systems are, the more likely they are to break down. Unfortunately, the unexpected breakdown may either incur a cost that is too high to be affordable (e.g. interruption of a space mission), or even worse, cause damage to users and their property due to close interactions with humans and environments. Therefore, faults of robotic systems must be taken care of properly in order to guarantee their safe operation. Procedures for dealing with faults include (i) detecting the occurrences of faults (fault detection), (ii) indicating faulty components (fault isolation), (iii) identifying features of faults (fault identification), and (iv) accommodating faults by dedicated control algorithms (fault tolerant control).

Fault detection and isolation (FDI) schemes have been investigated over the past three decades [1–3], and have been successfully applied to various safety-critical systems such as nuclear plants [4], flight control systems [5], vehicular drive-by-wire systems [6], automated highway systems [7,8], and robotic systems [9,10]. Commonly used techniques include state and parameter estimation [11–17], parity equations [18,19], neural networks [20,21], and multiple-model (MM) approaches [22–26]. On the other hand, fault tolerant control (FTC) can be realized with or without explicit FDI schemes [7,27–29]. In particular, applying FTC to robotic systems has drawn a lot of attention in the past [30–32].

In the aforementioned studies, faults are represented as either additive signals or multiple models. The former usually results in a complicated fault signal which is a function of the system state. Hence the fault signal cannot be treated as external disturbances, making it challenging to analyze and synthesize the FDI schemes. On the other hand, the latter represents each fault by a specific model that might be simple and structurally different from one another. Thus the multiple-model fault representation is more flexible and powerful, leading to the recent development of multiple-model FDI (MM–FDI) schemes.

For example, eight fault models were established for the air-intake system of a turbo-charged engine [22]; then structured hypothesis tests were used to detect the occurrences of faults. The multiple-model adaptive estimation (MMAE) algorithm, which runs parallel state estimators and calculates the probability of each model by Bayes' rule, has been applied to the flight control

* Corresponding author. Tel.: +886 3 5131249; fax: +886 3 5715998.
E-mail addresses: tshsiao@cn.nctu.edu.tw (T. Hsiao), mcw615@ymail.com (M.-C. Weng).

0921-8890/$ – see front matter © 2011 Elsevier B.V. All rights reserved.
doi:10.1016/j.robot.2011.10.003

system [33]. To improve the performance of multiple-model FDI (MM–FDI) schemes, the interacting multiple-model (IMM) algorithm was investigated [23] and applied to the satellite's attitude control system [24] as well as the aircraft lateral motion control system [25].

The aforementioned MM–FDI schemes enumerate all detectable and isolatable faults in the *model sets*. If an *unexpected* fault, i.e. a fault without a corresponding model in the model set, has occurred, the results of the MM–FDI schemes become unpredictable. Therefore, a large model set is required in order to detect and isolate as many faults as possible. Unfortunately, it is difficult, if not impossible, to design an exhaustive model set that contains every possible fault. Take the partial actuator fault [26] for example. The associated fault model incorporates a fixed multiplicative "effective factor" in the actuator's output, representing the reduction of the actuator's gain. Since the effective factor can be any number between 0 and 1, it is impossible to include all partial fault models in the model set. In fact, we are restricted to work on a finite model set, and we will show in Section 3 that expanding the model set results in a considerable increase of the computational load. Even though the computational load is affordable, a large model set is not recommended because some models may become indistinguishable from the input–output point of view, and then the MM–FDI schemes are unable to select the fittest model from the model set with "sufficient confidence". In short, MM–FDI schemes face a dilemma of avoiding unexpected faults by using a fine-grained model set while maintaining a tractable algorithm by limiting the size of the model set.

To tackle the model set design problem, Ru and Li [26] proposed the IM^{3}L algorithm that uses the IMM algorithm for estimating system state and the expectation-maximization (EM) algorithm for updating model parameters. Therefore the fault models are self-adaptive, relieving the need for a large model set. However only (multiple) abrupt total and partial faults were considered in [26].

In this paper, we propose a hierarchical multiple-model FDI (HMM-FDI) scheme as a solution to the model set design problem and apply it to detect and isolate actuator faults of robot manipulators. The ultimate goal of the proposed FDI scheme is to find out faulty joints in an early stage such that fault tolerant strategies can be launched in time to guarantee safe operation of the robotic system. In other words, any faulty joints must be indicated *before* the robotic system significantly deviates from its nominal performance, *no matter what kinds of faults have taken place*. To achieve this goal, the proposed HMM-FDI scheme works in stages. At each stage, the model set is refined such that only a small number of models are required. Therefore the HMM-FDI scheme avoids the need for enumerating all possible faults in the model set, while is endowed with the ability to detect and isolate various types of *unexpected* actuator faults, including abrupt faults, incipient faults, and simultaneous faults in a computationally efficient way. The relation between the fault detection stage of the HMM-FDI scheme and the likelihood ratio test is explicitly revealed and theoretical upper bounds of the false alarm and missed detection probabilities are evaluated. Then experiments are conducted to verify the performance and efficiency of the HMM-FDI scheme.

The remainder of this paper is organized as follows: Section 2 introduces the dynamic and kinematic models of the robot manipulator. Section 3 illustrates the notions of the MM–FDI methods and the related techniques. The HMM-FDI scheme is proposed in Section 4 while experimental results are presented in Section 5. Section 6 concludes this paper.

2. Dynamic and kinematic models of the manipulator

The dynamic equation of an n-joint manipulator is given as follows [34]:

$$\mathbf{M}(\mathbf{q}(t))\ddot{\mathbf{q}}(t) + \mathbf{C}(\mathbf{q}(t), \dot{\mathbf{q}}(t))\dot{\mathbf{q}}(t) + \mathbf{G}(\mathbf{q}(t)) + \mathbf{F}(\dot{\mathbf{q}}(t)) = \boldsymbol{\tau}(t) \quad (1)$$

where $\mathbf{q}(t), \dot{\mathbf{q}}(t), \ddot{\mathbf{q}}(t) \in \mathbb{R}^n$ are vectors of joint positions, velocities, and accelerations at time t, respectively. $\mathbf{M}(\mathbf{q}(t))$, $\mathbf{C}(\mathbf{q}(t), \dot{\mathbf{q}}(t)) \in \mathbb{R}^{n\times n}$ are the inertia matrix, and Coriolis and centrifugal matrix respectively. $\mathbf{G}(\mathbf{q}(t))$, $\mathbf{F}(\dot{\mathbf{q}}(t))$, $\boldsymbol{\tau}(t) \in \mathbb{R}^n$ denote the gravitational torque vector, friction vector, and control torque vector, respectively. For clarity, we will drop the notational dependence of all variables on t as long as it leads to no confusion.

Define the state vector of the manipulator as $\mathbf{x} = [\mathbf{q}^T, \dot{\mathbf{q}}^T]^T$. Because the proposed HMM-FDI scheme will be derived in the discrete-time domain, we apply the Euler's method to convert (1) to its discrete-time counterpart and obtain the following state space representation:

$$\mathbf{x}_{k+1} = \mathbf{x}_k + h\begin{bmatrix}\dot{\mathbf{q}}_k \\ \mathbf{f}(\mathbf{x}_k, \boldsymbol{\tau}_k)\end{bmatrix} + \begin{bmatrix}\mathbf{w}_k^p \\ \mathbf{w}_k^v\end{bmatrix} \quad (2)$$

where $\mathbf{f}(\mathbf{x}_k, \boldsymbol{\tau}_k) = \mathbf{M}^{-1}(\mathbf{q}_k)\left[\boldsymbol{\tau}_k - \mathbf{C}(\mathbf{q}_k, \dot{\mathbf{q}}_k)\dot{\mathbf{q}}_k - \mathbf{G}(\mathbf{q}_k) - \mathbf{F}(\dot{\mathbf{q}}_k)\right]$, h is the sampling time, and the subscript k denotes the kth sample. $\mathbf{w}_k = [(\mathbf{w}_k^p)^T, (\mathbf{w}_k^v)^T]^T$ is the process noise representing the model uncertainties and the approximation error due to the Euler's method.

We assume that only the joint positions are measurable. Thus the output equation of the manipulator is:

$$\mathbf{y}_k = \mathbf{C}\mathbf{x}_k + \mathbf{v}_k \quad (3)$$

where $\mathbf{C} = [\mathbf{I}_{n\times n}\mathbf{0}_{n\times n}]$ and $\mathbf{v}_k$ is the measurement noise which is assumed to be Gaussian distributed white noise with zero mean and covariance matrix $\mathbf{R}$.

In the context of the HMM-FDI scheme, the *dynamic model* consists of (2) and (3) along with the assumption that $\mathbf{w}_k$ is Gaussian distributed noise with zero mean and covariance matrix $\mathbf{Q}_k^D$. In addition, we assume that components of $\mathbf{w}_k$ are mutually uncorrelated, i.e. $\mathbf{Q}_k^D$ is a diagonal matrix. Note that we allow the covariance matrix to be time-varying.

Remark 1. It should be noted that the actual distribution of $\mathbf{w}_k$ may not be Gaussian; nevertheless the dynamic model *assumes* that $\mathbf{w}_k$ is Gaussian distributed and mutually uncorrelated, and treats the covariance matrix $\mathbf{Q}_k^D$ as a *tunable parameter of the model*, not a *physical quantity of the robot*. By tuning $\mathbf{Q}_k^D$ we change the "accuracy" of the dynamic model. If $\mathbf{Q}_k^D$ is set to an inappropriate value, then the dynamic model behaves poorly in predicting the motion of the manipulator; however, it is our intention to reduce the "relative accuracy" of one model w.r.t. the others for the purpose of fault detection and isolation. See Section 4 for more details.

On the other hand, we can predict the motion of the manipulator through the *kinematic relations* of joints. By kinematic relation we mean that the joint velocity is the first derivative of the joint position. Approximating the kinematic relation by the Euler's method yields

$$\mathbf{q}_{k+1} = \mathbf{q}_k + h\dot{\mathbf{q}}_k + \boldsymbol{\xi}_k^p \quad (4)$$

where $\boldsymbol{\xi}_k^p$ is the approximation error due to the Euler's method. On the other hand, if the differentiation relation is approximated by the backward difference equation, then we have

$$\dot{\mathbf{q}}_{k+1} = \frac{\mathbf{q}_{k+1} - \mathbf{q}_k}{h} + \boldsymbol{\xi}_k^v = \frac{\left(\mathbf{q}_k + h\dot{\mathbf{q}}_k + \boldsymbol{\xi}_k^p\right) - \mathbf{q}_k}{h} + \boldsymbol{\xi}_k^v \quad (5)$$

where $\boldsymbol{\xi}_k^v$ is the approximation error due to the backward difference equation. Combining (4) and (5) yields the following equation:

$$\mathbf{x}_{k+1} = \mathbf{A}^K\mathbf{x}_k + \mathbf{G}^K\boldsymbol{\xi}_k \quad (6)$$

where $\mathbf{A}^K = \begin{bmatrix} \mathbf{I} & h\mathbf{I} \\ \mathbf{0} & \mathbf{I} \end{bmatrix}$, $\mathbf{G}^K = \begin{bmatrix} \mathbf{I} & \mathbf{0} \\ \frac{1}{h}\mathbf{I} & \mathbf{I} \end{bmatrix}$, and $\boldsymbol{\xi}_k = \begin{bmatrix} \boldsymbol{\xi}_k^p \\ \boldsymbol{\xi}_k^v \end{bmatrix}$. In the context of the HMM-FDI scheme, the *kinematic model*[1] consists of (6) and (3) along with the assumption that $\boldsymbol{\xi}_k$ is Gaussian distributed with zero mean and covariance matrix $\mathbf{Q}_k^K$. We also assume that the components of $\boldsymbol{\xi}_k$ are mutually uncorrelated, i.e. $\mathbf{Q}_k^K$ is a diagonal matrix. Here $\mathbf{Q}_k^K$ is also regarded as a tunable parameter of the kinematic model (c.f. Remark 1). In addition, we assume that $\mathbf{v}_k$, $\mathbf{w}_k$ and $\boldsymbol{\xi}_k$ are independent.

Furthermore, we can describe the motion of the ith joint by either (7) (dynamic equation) or (8) (kinematic equation) below and obtain a set of models with arbitrary combinations of (7) and (8) for the n joints.

$$\begin{bmatrix} q_{i,k+1} \\ \dot{q}_{i,k+1} \end{bmatrix} = \begin{bmatrix} q_{i,k} \\ \dot{q}_{i,k} \end{bmatrix} + h \begin{bmatrix} \dot{q}_{i,k} \\ f_i(\mathbf{x}_k, \boldsymbol{\tau}_k) \end{bmatrix} + \begin{bmatrix} w_{i,k}^p \\ w_{i,k}^v \end{bmatrix} \tag{7}$$

$$\begin{bmatrix} q_{i,k+1} \\ \dot{q}_{i,k+1} \end{bmatrix} = \begin{bmatrix} q_{i,k} \\ \dot{q}_{i,k} \end{bmatrix} + h \begin{bmatrix} \dot{q}_{i,k} \\ 0 \end{bmatrix} + \begin{bmatrix} \xi_{i,k}^p \\ \frac{1}{h}\xi_{i,k}^p + \xi_{i,k}^v \end{bmatrix} \tag{8}$$

where the symbol i in the first part of the subscript denotes the ith element of a vector.

To facilitate the presentation, we introduce the notation $K(i, j, \ldots)$ to denote a model that includes (8) for those joints inside the parentheses, and (7) for all the other joints. For example, if $n = 3$, then $K(1, 3)$ denotes the following model:

$$\begin{bmatrix} q_{1,k+1} \\ q_{2,k+1} \\ q_{3,k+1} \\ \dot{q}_{1,k+1} \\ \dot{q}_{2,k+1} \\ \dot{q}_{3,k+1} \end{bmatrix} = \begin{bmatrix} q_{1,k} \\ q_{2,k} \\ q_{3,k} \\ \dot{q}_{1,k} \\ \dot{q}_{2,k} \\ \dot{q}_{3,k} \end{bmatrix} + h \begin{bmatrix} \dot{q}_{1,k} \\ \dot{q}_{2,k} \\ \dot{q}_{3,k} \\ 0 \\ f_2(\mathbf{x}_k, \boldsymbol{\tau}_k) \\ 0 \end{bmatrix} + \begin{bmatrix} \xi_{1,k}^p \\ w_{2,k}^p \\ \xi_{3,k}^p \\ \frac{1}{h}\xi_{1,k}^p + \xi_{1,k}^v \\ w_{2,k}^v \\ \frac{1}{h}\xi_{3,k}^p + \xi_{3,k}^v \end{bmatrix}.$$

In particular, (6) and (2) are denoted by $K(1, 2, \ldots, n)$ and $K(0)$ respectively.

3. Multiple-model FDI schemes

MM–FDI schemes use one model for one particular fault. Then all fault models as well as the normal model (2), i.e. the model describing the normal operation of the robot, are contained in a model set. Whenever a fault has taken place, the model that best fits the current behavior of the robot switches from the normal model to the associated fault model. If we can detect the switch of models and identify the associated fault model, the FDI problem is solved.

We say that the robotic system is currently in mode i if the ith model is the fittest one. Suppose that we have defined an *exclusive* and *exhaustive* model set which consists of J models. Namely, the robotic system is in one and exactly one of the J modes at any time. Then we can estimate the current mode of the robotic system by evaluating the probabilities of the modes.

[1] In the context of robotics, the term "kinematic model" usually refers to the transformation among the reference frames of joints or the transformation between the joint space and the task space. In this paper, the kinematic model refers to a model exploiting only the very fundamental relation between positions and velocities. The same idea has also been explored by other researchers in designing the kinematic Kalman filter (KKF) of manipulators [35].

Let $P(M_k^i)$ be the probability of the event M_k^i, which denotes that the robotic system is in mode i at step k for $i = 1, 2, \ldots, J$ and all k. We assume that M_k^i forms a Markov chain, i.e.

$$P(M_{k+1}^j | M_k^i, M_{k-1}^{i_{k-1}}, \ldots, M_0^{i_0}) = P(M_{k+1}^j | M_k^i) = \pi^{i,j},$$
$$i_0, i_1, \ldots, i_{k-1},\ i, j = 1, 2, \ldots, J \text{ and } \forall k. \tag{9}$$

$\pi^{i,j}$ is the *mode transition probability* satisfying $\sum_{j=1}^J \pi^{i,j} = 1$ for all i. The *posterior mode probability* conditioning on all measurements up to step k is

$$s_k^i = P\left(M_k^i | \mathbf{y}_1, \mathbf{y}_2, \ldots, \mathbf{y}_k\right), \quad i = 1, 2, \ldots, J \text{ and } \forall k. \tag{10}$$

If $s_k^j = \max\left\{s_k^1, \ldots, s_k^J\right\}$, then we conclude that the robotic system is in mode $j$at step k. Furthermore, if mode j is associated with a particular fault, then we infer that the corresponding fault has taken place. Therefore the FDI problem is equivalent to evaluating the posterior mode probabilities.

Evaluation of the posterior mode probabilities requires state estimation in the multiple-model setting. Related techniques adopted in this paper are introduced in the following subsections.

3.1. Nonlinear state estimation

Without loss of generality, we can assume that the ith model in the model set has the following state space representation:

$$\begin{aligned} \mathbf{x}_{k+1}^i &= \boldsymbol{\phi}^i(\mathbf{x}_k^i, \boldsymbol{\tau}_k) + \mathbf{w}_k^i \\ \mathbf{y}_k &= \mathbf{C}\mathbf{x}_k^i + \mathbf{v}_k, \end{aligned} \quad i = 1, \ldots, J \text{ and } \forall k$$

where $\boldsymbol{\phi}^i$ is a nonlinear function of the state $\mathbf{x}_k^i$ and the control torque $\boldsymbol{\tau}_k$; $\mathbf{w}_k^i$ and $\mathbf{v}_k$ are process noise and measurement noise respectively which are assumed to be Gaussian distributed with zero means and covariance matrices $\mathbf{Q}_k^i$ and $\mathbf{R}$.

In this paper, we use unscented Kalman filter (UKF) for nonlinear state estimation because in general, UKF achieves a better performance than the well-known extended Kalman filter (EKF) with similar computational complexity [36]. For completeness, the UKF algorithm is presented in Algorithm 1, where the following notations are used:

$$\hat{\mathbf{x}}_{k|t}^i = E\left[\mathbf{x}_k^i | \mathbf{y}_1, \ldots, \mathbf{y}_t\right], \qquad \mathbf{P}_{k|t}^i = \mathrm{var}\left(\mathbf{x}_k^i | \mathbf{y}_1, \mathbf{y}_2, \ldots, \mathbf{y}_t\right),$$
$$L_k = p\left(\mathbf{y}_k | \mathbf{y}_1, \mathbf{y}_2, \ldots, \mathbf{y}_{k-1}\right).$$

Algorithm 1: UKF algorithm

$(\hat{\mathbf{x}}_{k+1|k+1}^j, \mathbf{P}_{k+1|k+1}^j, L_{k+1}^j) =$
$\mathbf{UKF}(\hat{\mathbf{x}}_{k|k}^j, \mathbf{P}_{k|k}^j, \mathbf{y}_{k+1}, \boldsymbol{\tau}_k, \boldsymbol{\phi}^j, \mathbf{C}, \mathbf{Q}_k^j, \mathbf{R})$
{
$\boldsymbol{\chi}_0 = \hat{\mathbf{x}}_{k|k}^j$, $W_0 = \kappa/(N + \kappa)$ /* the dimension of $\mathbf{x}_k^j$ is $N = 2n$*/
$\boldsymbol{\chi}_i = \hat{\mathbf{x}}_{k|k}^j \pm \sqrt{n + \kappa}\left(\mathbf{P}_{k|k}^j\right)_i^{1/2}$, $W_i = 1/(2(N + \kappa))$,
$i = 1, 2, \ldots, 2N$
/* κ is a design parameter. $\mathbf{P}_{k|k}^j = \left(\mathbf{P}_{k|k}^j\right)^{1/2}\left(\mathbf{P}_{k|k}^j\right)^{T/2}$ and $\left(\mathbf{P}_{k|k}^j\right)_i^{1/2}$ is the ith column of $\left(\mathbf{P}_{k|k}^j\right)^{1/2}$ */
$\bar{\boldsymbol{\chi}}_i = \boldsymbol{\phi}^j(\boldsymbol{\chi}_i, \boldsymbol{\tau}_k)$, $\boldsymbol{\mu}_{k+1}^j = \sum_{i=0}^{2N} W_i \mathbf{C}\bar{\boldsymbol{\chi}}_i$
$\hat{\mathbf{x}}_{k+1|k}^j = \sum_{i=0}^{2N} W_i \bar{\boldsymbol{\chi}}_i$,
$\mathbf{P}_{k+1|k}^j = \sum_{i=0}^{2N} W_i \left(\bar{\boldsymbol{\chi}}_i - \hat{\mathbf{x}}_{k+1|k}^j\right)\left(\bar{\boldsymbol{\chi}}_i - \hat{\mathbf{x}}_{k+1|k}^j\right)^T + \mathbf{Q}_k^j$
$\mathbf{S}_{k+1}^j = \sum_{i=0}^{2N} W_i \left(\mathbf{C}\bar{\boldsymbol{\chi}}_i - \boldsymbol{\mu}_{k+1}^j\right)\left(\mathbf{C}\bar{\boldsymbol{\chi}}_i - \boldsymbol{\mu}_{k+1}^j\right)^T + \mathbf{R}$,
$\mathbf{P}_{xy} = \sum_{i=0}^{2N} W_i \left(\bar{\boldsymbol{\chi}}_i - \hat{\mathbf{x}}_{k+1|k}^j\right)\left(\mathbf{C}\bar{\boldsymbol{\chi}}_i - \boldsymbol{\mu}_{k+1}^j\right)^T$

(continued on next page)

$$\hat{\mathbf{x}}^j_{k+1|k+1} = \hat{\mathbf{x}}^j_{k+1|k} + \mathbf{P}_{xy}\mathbf{P}^{-1}_{yy}\left(\mathbf{y}_{k+1} - \boldsymbol{\mu}^j_{k+1}\right),$$
$$\mathbf{P}^j_{k+1|k+1} = \mathbf{P}^j_{k+1|k} - \mathbf{P}_{xy}\left(\mathbf{S}^j_{k+1}\right)^{-1}\mathbf{P}^T_{xy}$$
$$L^j_{k+1} = \frac{1}{(2\pi)^{\frac{n}{2}}\sqrt{\det \mathbf{S}^j_{k+1}}}$$
$$\exp\left\{-\frac{1}{2}\left(\mathbf{y}_{k+1} - \boldsymbol{\mu}^j_{k+1}\right)^T\left(\mathbf{S}^j_{k+1}\right)^{-1}\left(\mathbf{y}_{k+1} - \boldsymbol{\mu}^j_{k+1}\right)\right\}$$
}

$E[\cdot]$ and var(.) denote the expected value and variance respectively. $p(\cdot)$ is the probability density function (PDF). Comprehensive discussions about UKF can be found in [37].

3.2. Multiple-model state estimation

Given that the robotic system is in mode j, we can apply Algorithm 1 to estimate the state. Unfortunately, the mode of the robotic system is unknown; therefore the generalized pseudo-Bayesian method of order 2 (GPB-2) [38] is applied to estimate the state and the posterior mode probabilities in the multiple-model setting. Suppose that there are J models in the model set and define

$$\hat{\mathbf{x}}^{i,j}_{k|t} = E\left[\mathbf{x}_k | M^i_{k-1}, M^j_k, \mathbf{y}_1, \ldots, \mathbf{y}_t\right],$$
$$\mathbf{P}^{i,j}_{k|t} = \mathrm{var}\left(\mathbf{x}_k | M^i_{k-1}, M^j_k, \mathbf{y}_1, \ldots, \mathbf{y}_t\right)$$
$$L^{i,j}_k = p\left(\mathbf{y}_k | M^i_{k-1}, M^j_k, \mathbf{y}_1, \ldots, \mathbf{y}_{k-1}\right), \quad i, j = 1, \ldots, J. \tag{11}$$

Algorithm 2: GPB-2 algorithm

GPB2 /* Given $\hat{\mathbf{x}}^i_{k|k}$, $\mathbf{P}^i_{k|k}$ and s^i_k, GPB2 calculates $\hat{\mathbf{x}}^i_{k+1|k+1}$, $\mathbf{P}^i_{k+1|k+1}$, and s^i_{k+1} for $i = 1, 2, \ldots, J$ */
{
/* Run Algorithm 1 J^2 times. */
$(\hat{\mathbf{x}}^{i,j}_{k+1|k+1}, \mathbf{P}^{i,j}_{k+1|k+1}, L^{i,j}_{k+1}) =$
UKF$(\hat{\mathbf{x}}^i_{k|k}, \mathbf{P}^i_{k|k}, \mathbf{y}_{k+1}, \boldsymbol{\tau}_k, \boldsymbol{\phi}^j, \mathbf{C}, \mathbf{Q}^j_k, \mathbf{R})$; $i, j = 1, 2, \ldots, J$
$\left(\{\hat{\mathbf{x}}^i_{k+1|k+1}\}^J_{i=1}, \{\mathbf{P}^i_{k+1|k+1}\}^J_{i=1}, \{s^i_{k+1}\}^J_{i=1}\right) =$
Merging$\left(\{\hat{\mathbf{x}}^{i,j}_{k+1|k+1}\}^J_{i,j=1}, \{\mathbf{P}^{i,j}_{k+1|k+1}\}^J_{i,j=1}, \{L^{i,j}_{k+1}\}^J_{i,j=1}, \{s^i_k\}^J_{i=1}\right)$;
}
where
$\left(\{\hat{\mathbf{x}}^i_{k+1|k+1}\}^J_{i=1}, \{\mathbf{P}^i_{k+1|k+1}\}^J_{i=1}, \{s^i_{k+1}\}^J_{i=1}\right) =$
Merging$\left(\{\hat{\mathbf{x}}^{i,j}_{k+1|k+1}\}^J_{i,j=1}, \{\mathbf{P}^{i,j}_{k+1|k+1}\}^J_{i,j=1}, \{L^{i,j}_{k+1}\}^J_{i,j=1}, \{s^i_k\}^J_{i=1}\right)$
{
$s^{i,j}_{k,k+1} = \frac{L^{i,j}_{k+1}\pi^{i,j}s^i_k}{\sum^J_{i=1}\sum^J_{j=1}L^{i,j}_{k+1}\pi^{i,j}s^i_k}$, $s^j_{k+1} = \sum^J_{i=1}s^{i,j}_{k,k+1}$, $\hat{\mathbf{x}}^j_{k+1|k+1} = \frac{1}{s^j_{k+1}}\sum^J_{i=1}s^{i,j}_{k,k+1}\hat{\mathbf{x}}^{i,j}_{k+1|k+1}$, $i, j = 1, \ldots, J$
$\mathbf{P}^j_{k+1|k+1} = \frac{1}{s^j_{k+1}}\sum^J_{i=1}s^{i,j}_{k+1}\left[\mathbf{P}^{i,j}_{k+1|k+1} + \tilde{\mathbf{x}}^{i,j}_{k+1}(\tilde{\mathbf{x}}^{i,j}_{k+1})^T\right]$,
where $\tilde{\mathbf{x}}^{i,j}_{k+1} = \hat{\mathbf{x}}^j_{k+1|k+1} - \hat{\mathbf{x}}^{i,j}_{k+1|k+1} j = 1, \ldots, J$
}

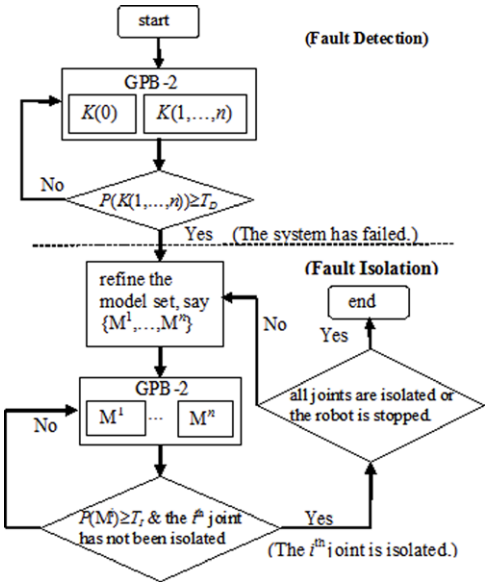

Fig. 1. Flowchart of the HMM-FDI scheme.

At each time step, the GPB-2 algorithm runs UKF J^2 times and generates J^2 state estimates $\hat{\mathbf{x}}^{i,j}_{k|k}$, $i, j = 1, \ldots, J$. $\hat{\mathbf{x}}^{i,j}_{k|k}$ denotes the estimated state under the condition that the robotic system switches from mode i to mode j at step k. In the meanwhile, the GPB-2 algorithm also evaluates the posterior mode probabilities (10). Then these J^2 state estimates are merged together according to the posterior mode probabilities, leaving J estimated states at the end of each step. The GPB-2 algorithm is presented in Algorithm 2.

4. HMM-FDI scheme

As we have mentioned in Section 1, model set design is the most challenging part of the MM–FDI approaches. To solve this problem, we propose to perform FDI in stages with mixture models of dynamic equations (7) and kinematic equations (8), resulting in a hierarchical multiple-model FDI (HMM-FDI) scheme. Unlike conventional MM–FDI approaches which detect and isolate faults in one step with a large model set, the proposed HMM-FDI scheme detects (multiple) faults as the first step, and then isolates the faulty joints as the next step. If the joints fail successively, the HMM-FDI scheme keeps refining its model set in the isolation stage until all faults have been isolated, or the robot is forced to give up its task. The flowchart of the HMM-FDI scheme is shown in Fig. 1.

4.1. Fault detection

In the fault detection stage, the model set consists of only two models: the dynamic model (2) and the kinematic model (6). Roughly speaking, we tune the model parameters $\mathbf{Q}^D_k$ and $\mathbf{Q}^K_k$ such that the dynamic model is more accurate than the kinematic model under normal operation. In other words, we increase $\mathbf{Q}^K_k$ or decrease $\mathbf{Q}^D_k$ such that the covariance of the estimated state associated with the kinematic model becomes larger than that of the dynamic model. Thus the GPB-2 algorithm favors the dynamic model and assigns a higher posterior mode probability to it, indicating that the robotic system is normal.

In the event of actuator faults, the faulty joints no longer satisfy the dynamic model; however the kinematic model remains a good approximation to the motion of all joints because it has nothing to do with actuators' torques. Thus the posterior mode probability of the kinematic model increases. If it exceeds a predefined threshold

T_D, we assert the occurrence of faults. Note that $0 < T_D < 1$; hence T_D represents the least confidence level we must have when we claim that the robotic system is faulty.

4.2. Fault isolation

In the fault isolation stage, we focus on finding out the faulty joints instead of recognizing the types of faults, i.e. whether the joint is locked or suffers from partial loss of the output gain does not matter as long as we know that it has failed. For easy illustration, we temporarily assume that multiple faults take place successively, not simultaneously. Under this assumption, the proposed model set for fault isolation is $\{K(1), K(2), \ldots, K(n)\}$ (see Section 2 for an explanation of the notations). Suppose that the jth joint has failed. Because all models but $K(j)$ incorporate the dynamic equation (7) for the jth joint, $K(j)$ is least susceptible to the fault of the jth joint. Therefore $K(j)$ will be assigned the highest posterior mode probability. If the posterior mode probability of $K(j)$ exceeds a predefined threshold T_I, we assert that the jth joint has failed. Since $0 < T_I < 1$, T_I represents the least confidence level we must have to isolate the faulty joint.

Once the faulty joint has been isolated, the robotic system may continue its operation, reconfigure its mission, or make an emergency stop. The decision is made by the control system, which is beyond the scope of this paper. However, the FDI scheme must be ready for detecting and isolating succeeding faults as long as the robotic system remains operational. To do this, the HMM-FDI scheme refines its model set as $\{K(j), K(1, j), K(2, j), \ldots, K(j, n)\}$ after the fault of the jth joint has been isolated. The new model set contains n models and all of them have the kinematic equation (8) for the jth joint. $n-1$ models include one more kinematic equation for one of the remaining $n-1$ joints. Note that $K(j)$ is the model with the highest posterior mode probability in the previous stage. If no more faults take place, $K(j)$ will be selected. On the other hand, if the mth joint has failed, $m \neq j$, then by the same arguments we infer that $K(j, m)$ will be assigned the highest posterior mode probability. If the posterior mode probability exceeds the threshold T_I, the mth joint is isolated. The process continues until the robotic system stops or all joints have been isolated.

Now we relax the assumption of no simultaneous faults. If any two joints may fail at the same time, the proposed model set is $\{K(i), K(i, j) | i, j = 1, \ldots, n\}$, i.e. the model set contains $C_1^n + C_2^n$ models that include kinematic equations for any one or any two joints. If the robot motion controller robustly alleviates the dynamic couplings of the joints [39], then the fault of one joint has minor effects on the other joints. Therefore $K(j)$ gets the highest posterior mode probability when a single fault occurs on the jth joint. This is because $K(j)$ includes the kinematic equation for the faulty joint and the more accurate dynamic equations for the other normal joints. Similarly, $K(i, j)$ gets the highest posterior mode probability when faults occur on the ith and jth joints simultaneously. Consequently, both single faults and simultaneous faults can be isolated. Then the model set is refined again. The refining procedure is similar: using the kinematic equations for all faulty joints, and one or two of the remaining normal joints.

Therefore we have established the procedure for FDI. Only two models are used for fault detection and a small number of models (depending on how many simultaneous faults are considered) are required for fault isolation. The refinement of the model set depends on the previously isolated faulty joints, and thus the evolution of the model set forms a hierarchical structure. Besides, no particular fault information (e.g. locked joints or partial loss of output gains) is assumed. Hence the HMM-FDI scheme is able to detect and isolate various types of *unexpected* actuator faults. Furthermore, the implementation of the HMM-FDI scheme can be computationally efficient in comparison with conventional MM–FDI approaches due to the reduced-sized model set. Experiments in Section 5 will verify the ability of the HMM-FDI scheme in immediate detection and isolation of a variety of actuator faults.

4.3. HMM-FDI scheme vs. likelihood ratio test

To analyze the performance of the HMM-FDI scheme, we relate its fault detection stage to the well-known *likelihood ratio test* and evaluate the probabilities of false alarms and missed detections. Recall that the *likelihood function* $L_k^{i,j}$ defined in (11) is the PDF of $\mathbf{y}_k$ conditioning on $\mathbf{y}_1, \ldots, \mathbf{y}_{k-1}$ as well as the mode transition from i to j at step k. Since only two models are involved in the fault detection stage, we use the superscript D and K to denote that the variable is evaluated based on the dynamic model and the kinematic model respectively.

According to Algorithms 1 and 2, $L_k^{i,j}$ is a Gaussian function with mean $\boldsymbol{\mu}_k^{i,j}$ and covariance matrix $\mathbf{S}_k^{i,j}$, $i, j = D, K$. However, the *true* likelihood function, i.e. the PDF of $\mathbf{y}_k$ conditioning on $\mathbf{y}_1, \ldots, \mathbf{y}_{k-1}$, is unknown and susceptible to faults. In the fault detection stage, let L_k^N and L_k^F denote the true likelihood functions under normal and faulty operations, respectively, i.e.

$$L_k^N = p\left(\mathbf{y}_k | \mathbf{y}_1, \ldots, \mathbf{y}_{k-1}, \text{ the system is normal at step } k\right)$$
$$L_k^F = p\left(\mathbf{y}_k | \mathbf{y}_1, \ldots, \mathbf{y}_{k-1}, \text{ the system is faulty at step } k\right).$$

L_k^N and L_k^F are unknown and may not be Gaussian. Their means and covariance matrices are denoted by $\boldsymbol{\mu}_k^N$, $\boldsymbol{\mu}_k^F$ and $\mathbf{S}_k^N$, $\mathbf{S}_k^F$, respectively and are unknown either. We explicitly distinguish $L_k^{i,j}$, $i = D, K$, from L_k^N and L_k^F to emphasize the difference between *models* and the *physical system*, especially when the accuracy of the models are reduced purposely.

If we choose

$$\mathbf{Q}_k^i = \begin{bmatrix} \mathbf{Q}_{11,k} & \mathbf{0} \\ \mathbf{0} & \mathbf{Q}_{22,k}^i \end{bmatrix}, \quad i = D, K, \text{ and all } k \tag{12}$$

where $\mathbf{Q}_{11,k}, \mathbf{Q}_{22,k}^i \in \mathbb{R}^{n \times n}$ are diagonal matrices, then direct computation based on the UKF algorithm yields $\boldsymbol{\mu}_k^{i,D} = \boldsymbol{\mu}_k^{i,K} \triangleq \boldsymbol{\mu}_k^i$, and $\mathbf{S}_k^{i,D} = \mathbf{S}_k^{i,K} \triangleq \mathbf{S}_k^i$, $i = D, K$. Therefore $L_k^{i,D}(\mathbf{y}_k) = L_k^{i,K}(\mathbf{y}_k) \triangleq L_k^i(\mathbf{y}_k)$ for $i = D, K$, and all $\mathbf{y}_k$. Furthermore, if we choose the mode transition probabilities defined in (9) to be $\pi^{D,D} = \pi^{K,K} = \pi^0$, then the GPB-2 algorithm leads to the following fault detection criterion:

The fault is detected at step $k \Leftrightarrow s_k^K \geq T_D \Leftrightarrow \frac{s_{k-1}^K L_k^K}{s_{k-1}^D L_k^D} \geq \frac{\pi^0 - (1 - T_D)}{\pi^0 - T_D} \Leftrightarrow \upsilon_k \geq r$ where $\upsilon_k = \rho_{k-1} + l_k$, $\rho_{k-1} = \log \frac{s_{k-1}^K}{s_{k-1}^D}$, $l_k = \log \frac{L_k^K}{L_k^D}$, and $r = \log \frac{\pi^0 - (1 - T_D)}{\pi^0 - T_D}$.

l_k is the log likelihood ratio of the kinematic model to the dynamic model. Therefore if (12) holds, the fault detection stage of the HMM-FDI scheme is equivalent to the likelihood ratio test with a time-varying threshold $r - \rho_{k-1}$, which depends on the ratio of posterior mode probabilities at the previous step.

Let P_k^{MD} and P_k^{FA} denote the probabilities of *missed detections* and *false alarms* at step k, respectively. Suppose that $\Re_k = \{\mathbf{y}_k \in \mathbb{R}^n | \upsilon_k(\mathbf{y}_k) < r\}$ is the set of outputs that do not trigger the alarm. $\Re_k^C$ is the complement of $\Re_k$. Then P_k^{MD} and P_k^{FA} are:

$$\begin{aligned} P_k^{MD} &= P\left(\Re_k | \text{ the system has failed}, \mathbf{y}_1, \ldots, \mathbf{y}_{k-1}\right) \\ &= \int_{\Re_k} L_k^F d\mathbf{y}_k = \int 1_{\Re_k} L_k^F d\mathbf{y}_k = E^F\left[1_{\Re_k}\right] \\ P_k^{FA} &= P\left(\Re_k^C | \text{ the system is normal}, \mathbf{y}_1, \ldots, \mathbf{y}_{k-1}\right) \\ &= \int_{\Re_k^C} L_k^N d\mathbf{y}_k = 1 - E^N\left[1_{\Re_k}\right] \end{aligned}$$

where 1_S is the indicator function of the set S, i.e. $1_S(\mathbf{y}_k) = 1$ if $\mathbf{y}_k \in S$, and $1_S(\mathbf{y}_k) = 0$ if $\mathbf{y}_k \notin S$. $E^i[\cdot]$ and $\mathrm{var}^i(\cdot)$ denote the mean and variance w.r.t. L_k^i, $i = N, F$. To further simplify the notations, we use E_k^i and V_k^i for $E^i[l_k]$ and $\mathrm{var}^i(l_k)$, $i = N, F$, respectively. Then the following theorem gives theoretical upper bounds of the false alarm and missed detection probabilities.

Theorem 1. *If (12) holds, and $\pi^0 > T_D > 0.5$, then*

$$P_k^{FA} \le \begin{cases} \bar{P}_k^{FA}, & E_k^N < r - \rho_{k-1} \\ 1, & E_k^N \ge r - \rho_{k-1}, \end{cases}$$

$$P_k^{MD} \le \begin{cases} \bar{P}_k^{MD}, & E_k^F > r - \rho_{k-1} \\ 1, & E_k^F \le r - \rho_{k-1} \end{cases}$$

where

$$\bar{P}_k^{FA} = 1 - \frac{1}{2r^2}\left\{(\rho_{k-1} + E_k^N - r)^2 + V_k^N + r^2 - \sqrt{[(\rho_{k-1} + E_k^N)^2 + V_k^N][(\rho_{k-1} + E_k^N - 2r)^2 + V_k^N]}\right\} < 1 \quad (13)$$

$$\bar{P}_k^{MD} = 1 - \frac{1}{2r^2}\left\{(\rho_{k-1} + E_k^F - r)^2 + V_k^F + r^2 - \sqrt{[(\rho_{k-1} + E_k^F)^2 + V_k^F][(\rho_{k-1} + E_k^F - 2r)^2 + V_k^F]}\right\} < 1. \quad (14)$$

Proof. We derive (13) in detail and (14) can be established by the same procedure.

Define $\mathfrak{M}_k = \{\mathbf{y}_k \in \mathbb{R}^n | \upsilon_k(\mathbf{y}_k) < 0\}$. Since $\pi^0 > T_D > 0.5$, r is positive. Therefore $\mathfrak{M}_k \subseteq \Re_k$, $\int_{\mathfrak{M}_k} \upsilon_k L_k^N d\mathbf{y}_k = E^N\left[1_{\mathfrak{M}_k}\upsilon_k\right] < 0$, and $\int_{\Re_k \setminus \mathfrak{M}_k} \upsilon_k L_k^N d\mathbf{y}_k \ge 0$. Besides, $E^N\left[1_{\mathfrak{M}_k}\right] \le E^N\left[1_{\Re_k}\right]$. Then

$$E^N[\upsilon_k] = \int_{\mathfrak{M}_k} \upsilon_k L_k^N d\mathbf{y}_k + \int_{\Re_k \setminus \mathfrak{M}_k} \upsilon_k L_k^N d\mathbf{y}_k + \int_{\Re_k^C} \upsilon_k L_k^N d\mathbf{y}_k \ge E^N\left[1_{\mathfrak{M}_k}\upsilon_k\right] + r\left(1 - E^N\left[1_{\Re_k}\right]\right). \quad (15)$$

Apply Cauchy–Schwarz inequality to $E^N\left[1_{\mathfrak{M}_k}\upsilon_k\right]$ and rearrange (15); then we obtain

$$\psi\left(\sqrt{E^N\left[1_{\Re_k}\right]}\right) \triangleq rE^N\left[1_{\Re_k}\right] + \sqrt{E^N\left[\upsilon_k^2\right]}\sqrt{E^N\left[1_{\Re_k}\right]} + \left(E^N[\upsilon_k] - r\right) \ge 0.$$

Note that ψ is a convex parabolic function of $\sqrt{E^N\left[1_{\Re_k}\right]}$. It is easy to show that ψ has two real roots and at least one of them is negative. Therefore if $E^N[\upsilon_k] \ge r$, both roots are negative, implying that $\psi \ge 0$ for all $0 \le E^N\left[1_{\Re_k}\right] \le 1$. On the other hand, if $E^N[\upsilon_k] < r$, then we can show that ψ has one positive root which is always less than 1. Under these circumstances, $\psi \ge 0$ implies

$$0 \le \frac{1}{2r}\left(-\sqrt{E\left[\upsilon_k^2\right]} + \sqrt{E^N\left[\upsilon_k^2\right] - 4r\left(E^N[\upsilon_k] - r\right)}\right) \le \sqrt{E^N\left[1_{\Re_k}\right]} \le 1. \quad (16)$$

Since $P_k^{FA} = 1 - E^N\left[1_{\Re_k}\right]$, $E^N[\upsilon_k] \ge r$ implies $P_k^{FA} \le 1$. In this case, we say that the upper bound is *trivial* because it provides little information about the false alarm probability. On the other hand, if $E^N[\upsilon_k] < r$, then (16) holds, implying $P_k^{FA} \le \bar{P}_k^{FA} < 1$. □

Note that $\bar{P}_k^{FA}$ is a function of E_k^N and V_k^N. It is straightforward to show that the partial derivatives of $\bar{P}_k^{FA}$ w.r.t. both E_k^N and V_k^N are always nonnegative, i.e. $\bar{P}_k^{FA}$ is a non-decreasing function of E_k^N and V_k^N. Hence if $E_k^N \le \bar{E}_k^N$ and $V_k^N \le \bar{V}_k^N$, then $\bar{P}_k^{FA}\left(E_k^N, V_k^N\right) \le \bar{P}_k^{FA}\left(\bar{E}_k^N, \bar{V}_k^N\right)$. An upper bound of E_k^i can be evaluated directly from its definition as follows:

$$E_k^i \le \frac{1}{2}\left(n \log \frac{\lambda_{n,k}^D}{\lambda_{1,k}^K} + \frac{\mathrm{tr}\mathbf{S}_k^i + \left\|\Delta\boldsymbol{\mu}_k^{iD}\right\|^2}{\lambda_{1,k}^D} - \frac{\mathrm{tr}\mathbf{S}_k^i + \left\|\Delta\boldsymbol{\mu}_k^{iK}\right\|^2}{\lambda_{n,k}^K}\right), \quad i = N, F \quad (17)$$

where $\lambda_{1,k}^i$ and $\lambda_{n,k}^i$ are the minimum and maximum eigenvalues of $\mathbf{S}_k^i$ respectively; $\Delta\boldsymbol{\mu}_k^{ji} = \boldsymbol{\mu}_k^j - \boldsymbol{\mu}_k^i$ for $i = D, K$ and $j = N, F$. $\|\cdot\|$ is the Euclidean norm and tr• is the trace of a matrix. Furthermore, if L_k^N and L_k^F are Gaussian functions, then an upper bound of V_k^i can be found as follows [40]:

$$V_k^i \le \left(\mathrm{tr}\mathbf{S}_k^i\right)^2\left(\frac{1}{\lambda_{1,k}^D} + \frac{1}{\lambda_{1,k}^K}\right)^2 + \mathrm{tr}\mathbf{S}_k^i\left(\frac{\left\|\Delta\boldsymbol{\mu}_k^{iD}\right\|}{\lambda_{1,k}^D} + \frac{\left\|\Delta\boldsymbol{\mu}_k^{iK}\right\|}{\lambda_{1,k}^K}\right)^2, \quad i = N, F. \quad (18)$$

Substitute (17) and (18) into (13) and (14), and we can find the theoretical upper bounds of the false alarm and missed detection probabilities in terms of parameters of the models, i.e. $\lambda_{1,k}^i$, $\lambda_{n,k}^i$ and $\boldsymbol{\mu}_k^i$, $i = D, K$, and parameters of the physical system, i.e. $\mathrm{tr}\mathbf{S}_k^j$ and $\boldsymbol{\mu}_k^j$, $j = N, F$.

Remark 2. (18) holds under the assumption that L_k^i is a Gaussian function, $i = N, F$. However it is also possible to find an upper bound of V_k^i w.r.t. any other distributions [40]. We made the Gaussian assumption because it facilitates the derivation of the upper bound in terms of $\lambda_{1,k}^i$ and $\lambda_{n,k}^i$, $i = D, K$.

5. Experiments

5.1. Experimental setting

A two-joint manipulator was set up for experimental verifications. The schema and the photograph of the manipulator are shown in the left and right sides of Fig. 2 respectively. Each link is driven by a DC motor with an optical encoder mounted on the shaft. A motion controller and the HMM-FDI scheme are implemented on a 32-bit floating point DSP chip (TMS320F28335). The sampling time is 0.01 s. The dynamics of the DC motors and the manipulator can be lumped together as follows [34].

$$\underbrace{\begin{bmatrix} \theta_1 + \theta_2 + 2\theta_3\cos q_2 & \theta_2 + \theta_3\cos q_2 \\ \theta_7 + \theta_8\cos q_2 & \theta_7 + \theta_9 \end{bmatrix}}_{\bar{\mathbf{M}}(\mathbf{q})}\begin{bmatrix}\ddot{q}_1 \\ \ddot{q}_2\end{bmatrix} + \underbrace{\begin{bmatrix} -\theta_3\dot{q}_2\sin q_2 & -\theta_3(\dot{q}_1 + \dot{q}_2)\sin q_2 \\ \theta_8\dot{q}_1\sin q_2 & 0 \end{bmatrix}}_{\bar{\mathbf{C}}(\mathbf{q},\dot{\mathbf{q}})}\begin{bmatrix}\dot{q}_1 \\ \dot{q}_2\end{bmatrix} + \underbrace{\begin{bmatrix} \theta_4\cos q_1 + \frac{g}{l_1}\theta_3\cos(q_1 + q_2) \\ \frac{g}{l_1}\theta_8\cos(q_1 + q_2) \end{bmatrix}}_{\bar{\mathbf{G}}(\mathbf{q})} + \underbrace{\begin{bmatrix} \theta_5\dot{q}_1 + \theta_6\,\mathrm{sgn}\,\dot{q}_1 \\ \theta_{10}\dot{q}_1 + \theta_{11}\,\mathrm{sgn}\,\dot{q}_1 \end{bmatrix}}_{\bar{\mathbf{F}}(\dot{\mathbf{q}})} = \begin{bmatrix}\upsilon_1 \\ \upsilon_2\end{bmatrix} \quad (19)$$

where the control inputs υ_1 and υ_2 are armature voltages of the DC motors within the range of ±24 V. θ_i, $i = 1, 2, \ldots, 11$, are model

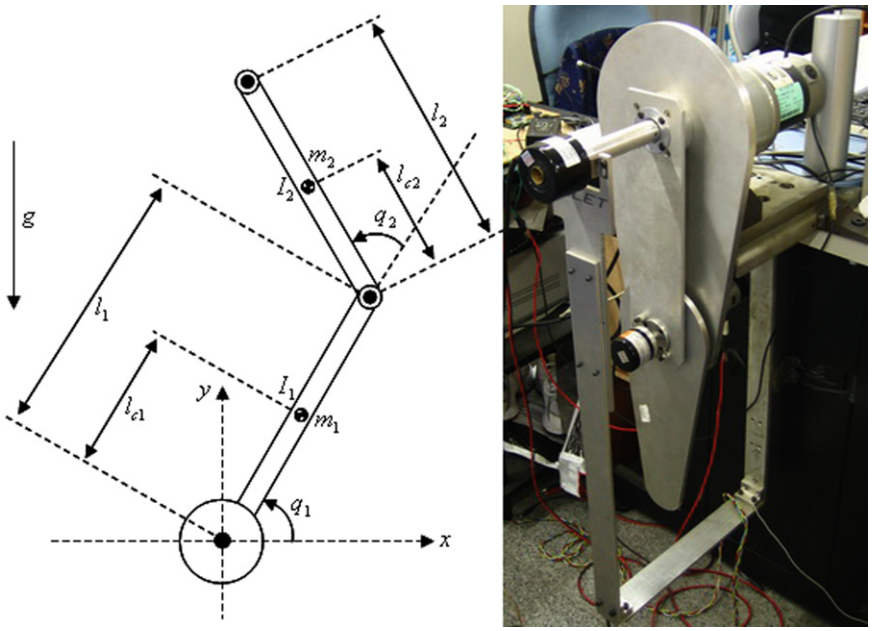

Fig. 2. (Left) Schema of the two-joint manipulator. (Right) Photograph of the manipulator.

Table 1
Model parameters and their nominal values.

$\theta_1 = [(I_1 + m_1 l_{c1}^2 + m_2 l_1^2)\frac{1}{r_1^2} + J_1]\frac{1}{k_1}$	0.3339		
$\theta_2 = (I_2 + m_2 l_{c2}^2)\frac{1}{r_1^2 k_1}$	0.0048	$\theta_3 = m_2 l_1 l_{c2}\frac{1}{r_1^2 k_1}$	0.0054
$\theta_4 = (m_1 l_{c1} + m_2 l_1) g \frac{1}{r_1^2}\frac{1}{k_1}$	2.1450	$\theta_5 = b_1 \frac{1}{k_1}$	2.8219
$\theta_6 = f_{c1}\frac{1}{r_1^2}\frac{1}{k_1}$	1.5177	$\theta_7 = (I_2 + m_2 l_{c2}^2)\frac{1}{r_2^2 k_2}$	0.0240
$\theta_8 = m_2 l_1 l_{c2}\frac{1}{r_2^2 k_2}$	0.0280	$\theta_9 = J_2\frac{1}{r_2^2 k_2}$	0.00002
$\theta_{10} = b_2\frac{1}{k_2}$	1.2211	$\theta_{11} = f_{c2}\frac{1}{r_2^2}\frac{1}{k_2}$	1.6282

Table 2
Nomenclature of the model parameters.

I_1, (I_2)	Moment of inertia of the 1st (2nd) link
m_1, (m_2)	Mass of the 1st (2nd) joint
l_1, (l_2)	Length of the 1st (2nd) joint
l_{c1}, (l_{c2})	Distance from the joint to the C.G. of the 1st (2nd) link
J_1, (J_2)	Inertia of the motor's rotor of the 1st (2nd) joint
r_1, (r_2)	Gear ratio of the 1st (2nd) joint
k_1, (k_2)	Lumped constants of motors in the 1st (2nd) joint
f_{c1}, (f_{c2})	Coulomb friction coefficients of the 1st (2nd) joint
b_1, (b_2)	Combined viscous friction coefficients
g	Gravity acceleration

parameters explained in Table 1. Their values are determined by the system identification techniques [41], and are given in Table 1 too. SI unit system is adopted for all physical quantities of the manipulator which are shown in Table 2.

A computed torque plus PID motion controller is implemented on the manipulator such that the joint position follows a desired trajectory. The controller has the following form:

$$\mathbf{v} = \bar{\mathbf{M}}(\mathbf{q})\left[\ddot{\mathbf{q}}_d + \mathbf{K}_v\dot{\tilde{\mathbf{q}}} + \mathbf{K}_p\tilde{\mathbf{q}} + \mathbf{K}_I\int\tilde{\mathbf{q}}dt\right] + \bar{\mathbf{C}}(\mathbf{q},\dot{\mathbf{q}})\dot{\mathbf{q}} + \bar{\mathbf{G}}(\mathbf{q}) + \bar{\mathbf{F}}(\dot{\mathbf{q}})$$

where $\mathbf{v} = [v_1, v_2]^T$ and the definitions of $\bar{\mathbf{M}}(\mathbf{q})$, $\bar{\mathbf{C}}(\mathbf{q},\dot{\mathbf{q}})$, $\bar{\mathbf{G}}(\mathbf{q})$, and $\bar{\mathbf{F}}(\dot{\mathbf{q}})$ are given in (19). $\mathbf{K}_v$, $\mathbf{K}_p$ and $\mathbf{K}_I$ are PID gain matrices which are tuned manually to achieve a satisfactory performance. The following values are used in the experiments:

$$\mathbf{K}_p = \mathrm{diag}(800, 500), \qquad \mathbf{K}_v = \mathrm{diag}(30, 15),$$
$$\mathbf{K}_I = \mathrm{diag}(1.411, 0.3).$$

In the experiments, the desired trajectory in the joint space is

$$q_{1d}(t) = -\frac{\pi}{2} + \frac{\pi}{4}(1 - e^{-2t^3}) + \frac{\pi}{9}(1 - e^{-2t^3})\sin(4t)$$
$$q_{2d}(t) = \frac{\pi}{3}(1 - e^{-2t^3}) + \frac{\pi}{6}(1 - e^{-2t^3})\sin(3t).$$

Remark 3. If a closed-loop system consists of both a controller and an FDI scheme, the FDI scheme is inevitably affected by the controller. A robust controller reduces the fluctuation of the system state caused by model uncertainties, external disturbances, and faults as well, making the closed-loop system less sensitive to faults. Moreover, some "soft faults", i.e. faults that are not detrimental to the system stability and performance, may turn out to be invisible from the input–output data due to the robustness of the controller. However, integrated design of the controller and the FDI scheme remains an open question and is beyond the scope of this paper. To carry out experiments, we implement the motion controller first and then manually tune the parameters of the HMM-FDI scheme. Despite the non-optimal combination of the controller and the FDI scheme, experimental results demonstrate that tracking performance of the control system just deteriorates slightly before the fault is detected and isolated. Hence we consider the performance of the HMM-FDI scheme satisfactory as far as the manipulator's safe operation is concerned.

In the fault detection stage, the model set consists of the dynamic model (2) and the kinematic model (6). In the fault isolation stage, the model set is chosen to be $\{K(1), K(2), K(1,2)\}$ such that simultaneous faults can be isolated. Since all combinations of faulty joints are included in the last model set, there is no need to refine it during the isolation stage. The following parameters of the HMM-FDI scheme are chosen: $\mathbf{R} = 0.001^2\mathbf{I}$, $\mathbf{Q}_{11,k} = 0.0026^2\mathbf{I}$, $\mathbf{Q}^D_{22,k} = 0.0023^2\mathbf{I}$, $\mathbf{Q}^K_{22,k} = 0.003^2\mathbf{I}$, for all k, $\pi^{D,D} = \pi^{K,K} = 0.999$, and $T_D = 0.7$, and $T_I = 0.75$. Five types of faults in Table 3 are considered. Note that Type 5 fault is an incipient fault indicating a gradual

Table 3
Five types of actuator faults.

Type	Description
Type 1	The 1st joint is locked.
Type 2	Both joints are locked simultaneously.
Type 3	The 1st joint is locked first; then the 2nd joint is locked.
Type 4	The 1st joint loses 60% of its output torque.
Type 5	The output torque of the 2nd joint gradually decays to zero with time constant 0.15 s.

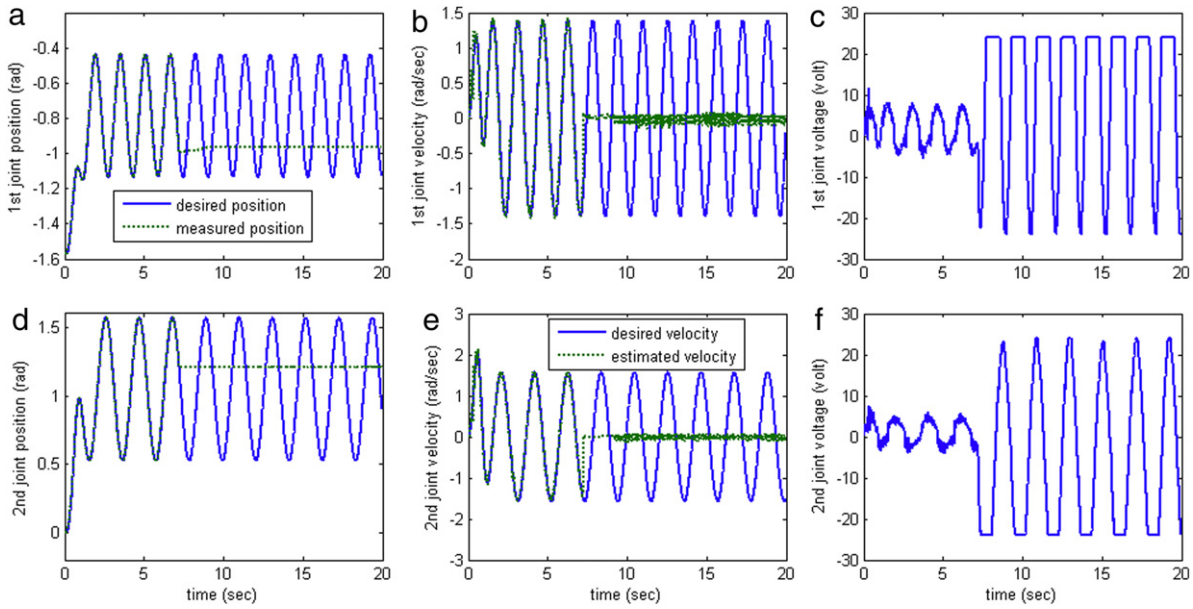

Fig. 3. The 1st joint is locked at $t = 10$ s. (a), (d) Joint positions: desired trajectory (solid line); real trajectory (dotted line). (b), (e) Joint velocities: desired velocities (solid line); estimated velocities (dotted line). (c), (f) Armature voltages of both joints.

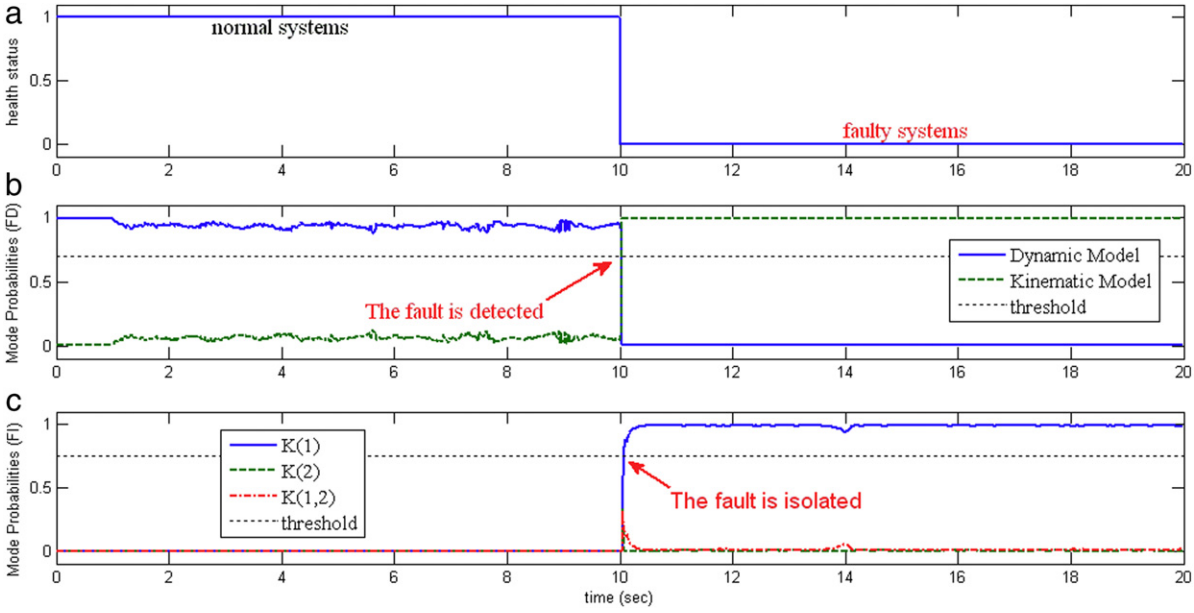

Fig. 4. (a) The fault occurs suddenly at $t = 10$ s. (b) Posterior mode probabilities of the dynamic model (solid line) and the kinematic model (dotted line). The fault is detected at $t = 10.04$ s. (c) Posterior mode probabilities of $K(1)$ (solid line), $K(2)$ (dashed line) and $K(1, 2)$ (dash–dot line). The faulty joint is isolated at $t = 10.08$ s.

loss of the actuator's torque. All the others are abrupt faults. Type 2 is simultaneous faults, Type 3 represents successive multiple faults, and all the others are single faults.

Note that it is difficult for the conventional MM–FDI methods to model Type 4 and Type 5 faults since both the percentage of loss and the time constant of the decay are unknown and may vary substantially. However, the HMM-FDI scheme can handle these faults easily. Even if the models for these five types of faults are established, the computational load is very demanding. Because the model set contains at least six models (five fault models and one normal model), the conventional MM–FDI methods have to run at least 36 UKFs at each sampling time. On the other hand, the

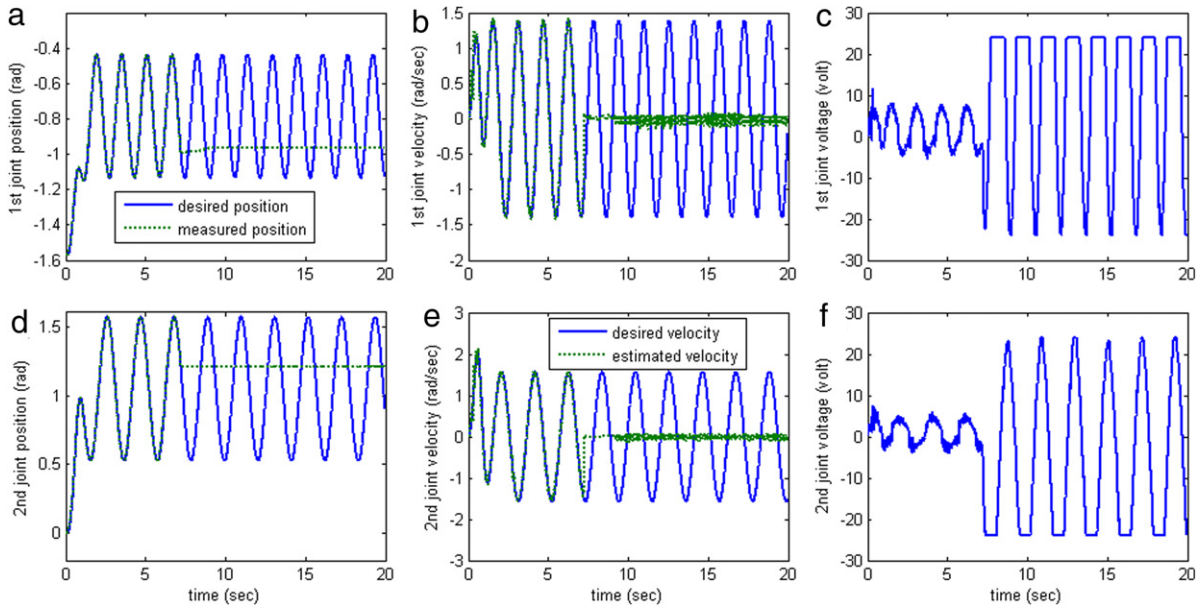

Fig. 5. Both joints are locked at $t = 7.2$ s. (a), (d) Joint positions: desired trajectory (solid line); real trajectory (dotted line). (b), (e) Joint velocities: desired velocities (solid line); estimated velocities (dotted line). (c), (f) Armature voltages of both joints.

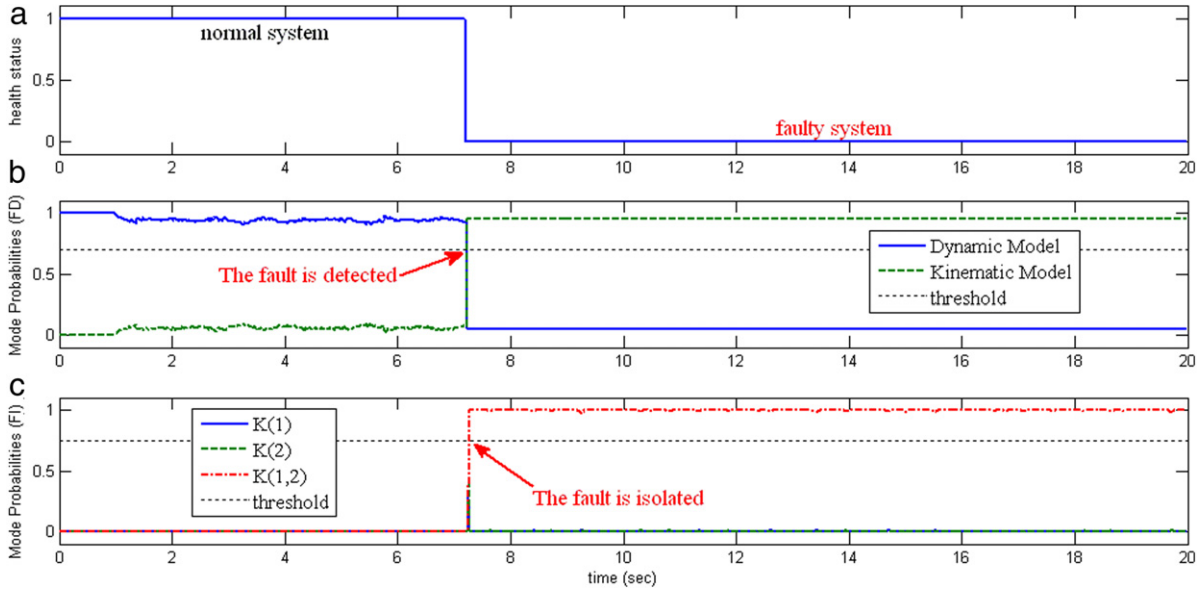

Fig. 6. (a) The fault occurs suddenly at $t = 7.2$ s. (b) Posterior mode probabilities of the dynamic model (solid line) and the kinematic model (dashed line). The fault is detected at $t = 7.23$ s. (c) Posterior mode probabilities of $K(1)$ (solid line), $K(2)$ (dashed line) and $K(1, 2)$ (dash–dot line). The faulty joint is isolated at $t = 7.28$ s.

HMM-FDI scheme uses at most three models in the model set and runs at most 9 UKFs at each sampling time. Therefore the HMM-FDI scheme not only extends the applicability of the conventional MM–FDI methods, but also significantly improves the computational efficiency. Besides, the HMM-FDI scheme does not incorporate any particular fault information in the models. Hence these five types of faults are all unexpected to the HMM-FDI scheme. However, the HMM-FDI scheme is not restricted to detecting and isolating only these five types of faults. More unexpected faults can be detected and isolated with the HMM-FDI scheme unaltered.

5.2. Experimental results

• *The* 1st *joint is locked* (*Type* 1)

Suppose that at $t = 10$ s, the first joint is suddenly locked. The results are shown in Figs. 3 and 4. Fig. 3 illustrates the positions, velocities, and armature voltages of both joints. It can be seen that the 1st joint is locked at $t = 10$ s while the 2nd joint operates normally. Since the dynamics of both joints are coupled, the 2nd joint is affected by the fault of the 1st joint. However, due to the robustness of the controller, the tracking performance of the 2nd joint just degrades slightly in the event of the locked 1st joint. It can also be seen from Fig. 3(b), (e) that the estimated velocities are close to the desired velocities, implying that the state estimators included in the HMM-FDI scheme work well.

The posterior mode probabilities for fault detection and fault isolation are shown in Fig. 4. During normal operation, the posterior mode probability of the dynamic model is significantly higher than that of the kinematic model. Therefore false alarms caused by model uncertainties and external disturbances are avoided. After the fault occurs, the posterior mode probability of the kinematic model dominates. It takes 0.04 s to detect the fault.

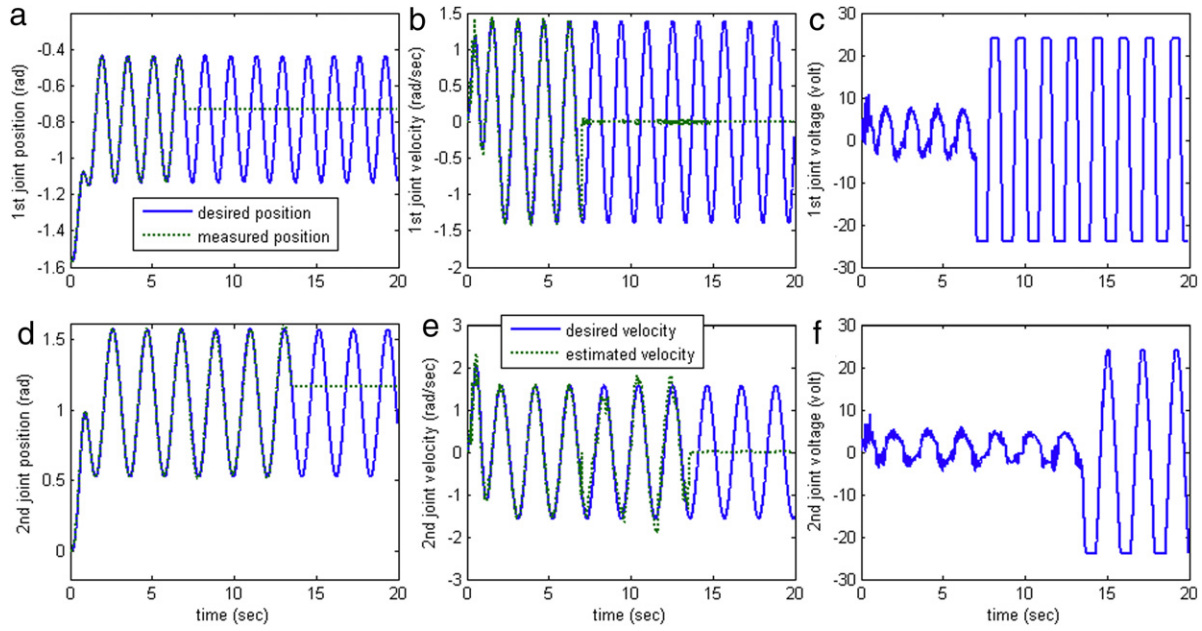

Fig. 7. The 1st joint is locked at $t = 7$ s and then the 2nd joint is locked at $t = 13.5$ s. (a), (d) Joint positions: desired trajectory (solid line); real trajectory (dotted line). (b), (e) Joint velocities: desired velocities (solid line); estimated velocities (dotted line). (c), (f) Armature voltages of both joints.

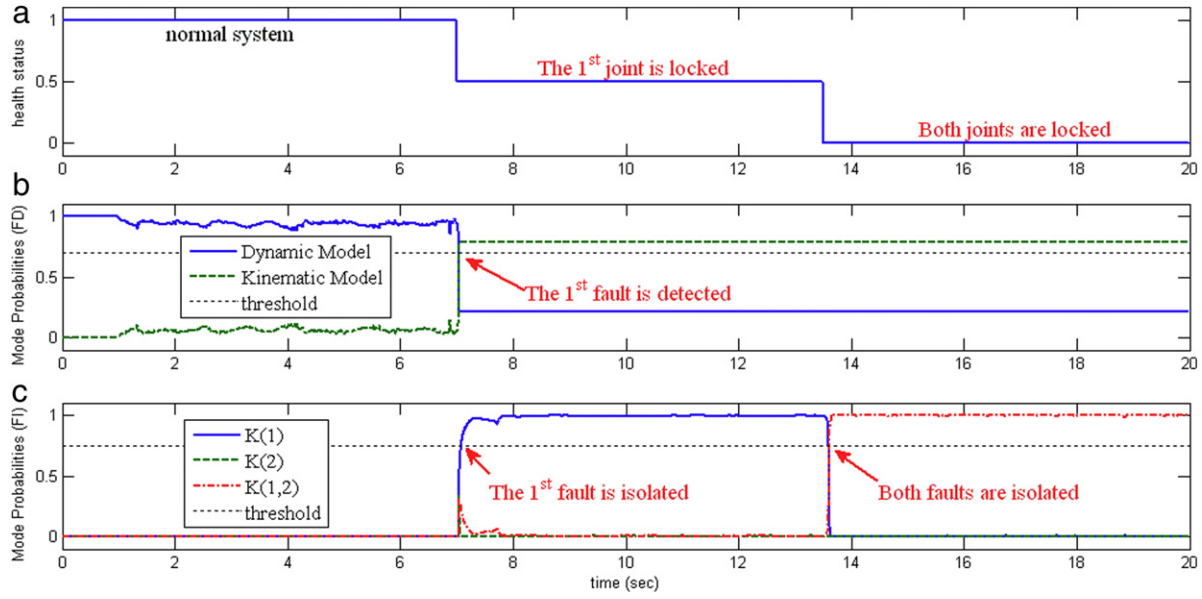

Fig. 8. (a) The first fault occurs suddenly at $t = 7.2$ s and then the second fault occurs suddenly at $t = 13.5$ s. (b) Posterior mode probabilities of the dynamic model (solid line) and the kinematic model (dashed line). The first fault is detected at $t = 7.23$ s. (c) Posterior mode probabilities of $K(1)$ (solid line), $K(2)$ (dashed line) and $K(1, 2)$ (dash–dot line). The first fault is isolated at $t = 7.28$ s. Then the second fault is isolated at $t = 13.61$ s.

Once the fault has been detected, the model set changes and the fault isolation process starts. The posterior mode probability of $K(1)$ becomes highest. The time between the occurrence of the fault and the time of the fault being isolated is 0.08 s.

• *Both joints are locked simultaneously* (*Type* 2)

Suppose that both joints are suddenly locked at $t = 7.2$ s. The positions, velocities, and armature voltages of both joints are shown in Fig. 5. Fig. 6 illustrates the posterior mode probabilities for fault detection and fault isolation. The HMM-FDI scheme detects and isolates the fault within 0.03 s and 0.08 s respectively.

• *Both joints are locked successively* (*Type* 3)

In this case, the 1st joint is locked at $t = 7$ s; then the 2nd joint is locked at $t = 13.5$ s. Fig. 7 illustrates the positions, velocities, and armature voltages of both joints. The posterior mode probabilities for fault detection and fault isolation are shown in Fig. 8. The fault of the 1st joint is detected and isolated within 0.03 s and 0.08 s respectively. At this moment, the model $K(1)$ has the highest probability since the 1st joint is locked. Then the 2nd joint is locked at $t = 13.5$ s and the model with highest probability switches to $K(1, 2)$ at $t = 13.61$ s, indicating that both joints have failed.

• *The* 1st *joint loses* 60% *of its output torque* (*Type* 4)

Suppose that the 1st joint suddenly loses 60% of its output torque at $t = 8$ s. The experimental results are shown in Figs. 9 and 10. We can see from Fig. 9 that this type of fault has minor effects on the tracking performance because the controller has compensated for the fault by increasing the armature voltage of the 1st joint after the fault has taken place.

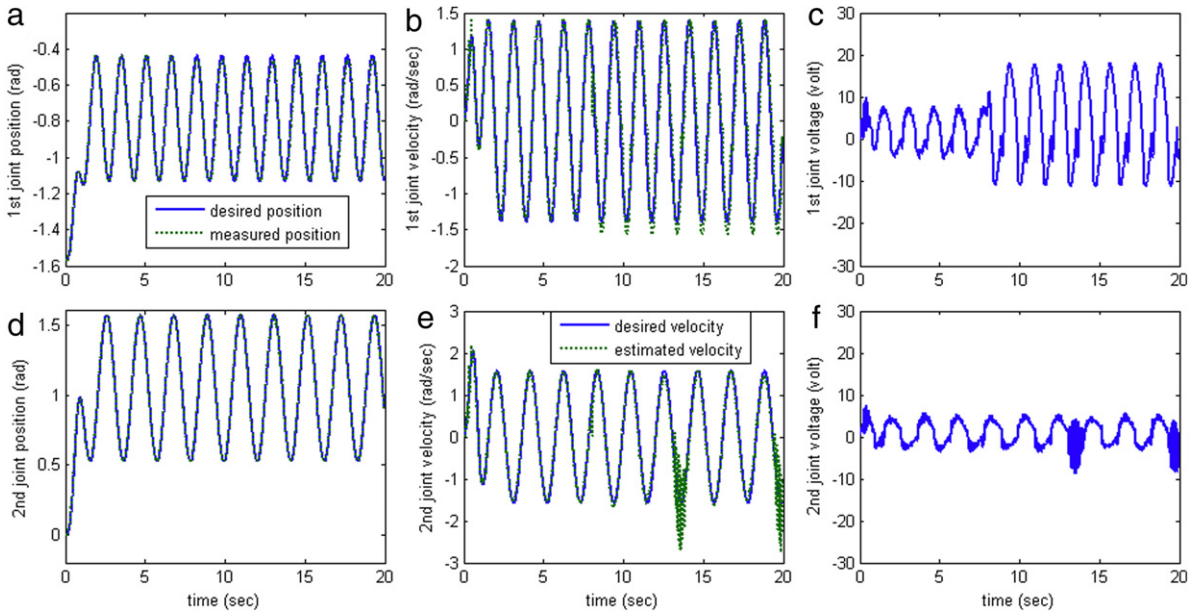

Fig. 9. The 1st joint loses 60% of its output torque at $t = 8$ s. (a), (d) Joint positions: desired trajectory (solid line); real trajectory (dotted line). (b), (e) Joint velocities: desired velocities (solid line); estimated velocities (dotted line). (c), (f) Armature voltages of both joints.

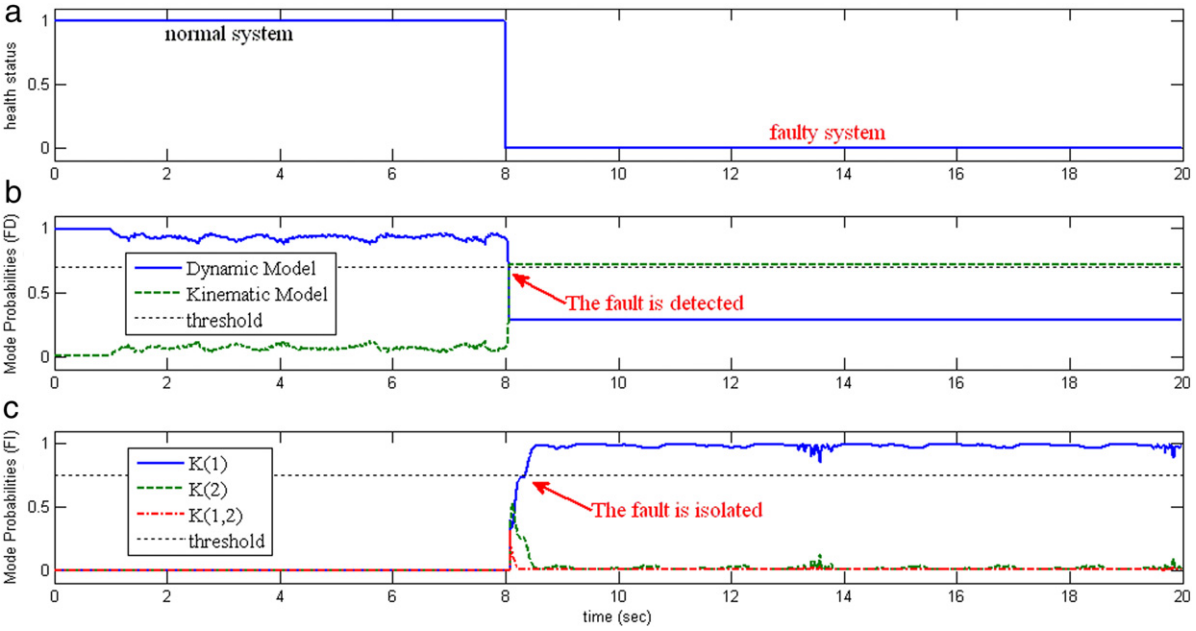

Fig. 10. (a) The fault occurs suddenly at $t = 8$ s. (b) Posterior mode probabilities of the dynamic model (solid line) and the kinematic model (dashed line). The fault is detected at $t = 8.07$ s. (c) Posterior mode probabilities of $K(1)$ (solid line), $K(2)$ (dashed line) and $K(1, 2)$ (dash–dot line). The faulty joint is isolated at $t = 8.37$ s.

The posterior mode probabilities are demonstrated in Fig. 10. The fault is detected and isolated within 0.07 s and 0.37 s respectively. Note that in the fault detection stage, the posterior mode probability of the kinematic model is just above the threshold T_D when Type 4 fault has taken place. Some readers may argue that if the loss of the output torque is less than 60%, the fault may be undetected and the sensitivity to faults of the HMM-FDI scheme is questionable. However the reason for not detecting the slight loss of the output torque is that the controller has already made compensation for it. In such a case, a slight loss of the output torque is usually regarded as model uncertainties due to underestimation of actuator gains, and should be taken care of by a robust controller. Instead, alarms triggered by small variations of actuator gains may be considered as false alarms.

• *The output torque of the* 2*nd joint gradually decays* (*Type* 5)

Suppose that the output torque of the 2nd joint gradually decays after $t = 7$ s. More precisely, let τ_2 be the output torque delivered by the controller to the 2nd joint, and τ_{2a} be the actual torque experienced by the 2nd link. For Type 5 fault, we assume that $\tau_{2a}(t) = e^{-0.15(t-7)}\tau_2(t)$ for $t \geq 7$. Experimental results are shown in Figs. 11 and 12.

Because the output torque of the 2nd joint gradually decays, the controller gradually increases the armature voltage of the 2nd joint to compensate for the loss of the control torque. The tracking performance degenerates slightly before the fault is detected (see Fig. 11). Consequently the HMM-FDI scheme takes a longer time to detect and isolate the fault (3.21 s and 3.51 s, respectively). However we consider the detection and isolation

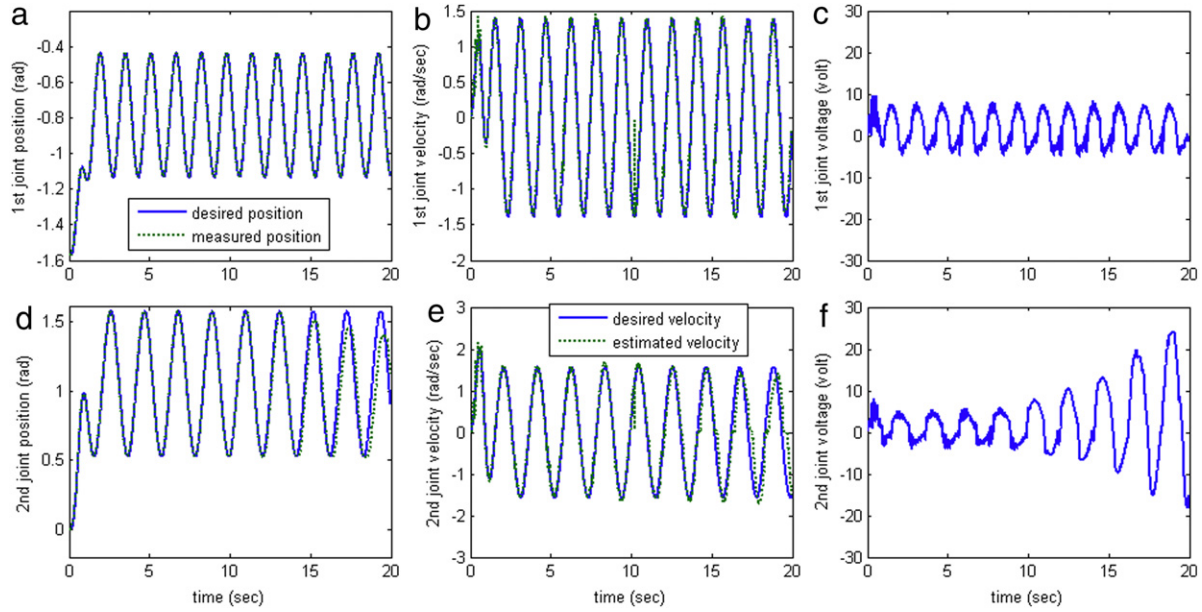

Fig. 11. The output torque of the 2nd joint gradually decay, starting at $t = 7$ s. (a), (d) Joint positions: desired trajectory (solid line); real trajectory (dotted line). (b), (e) Joint velocities: desired velocities (solid line); estimated velocities (dotted line). (c), (f) Armature voltages of both joints.

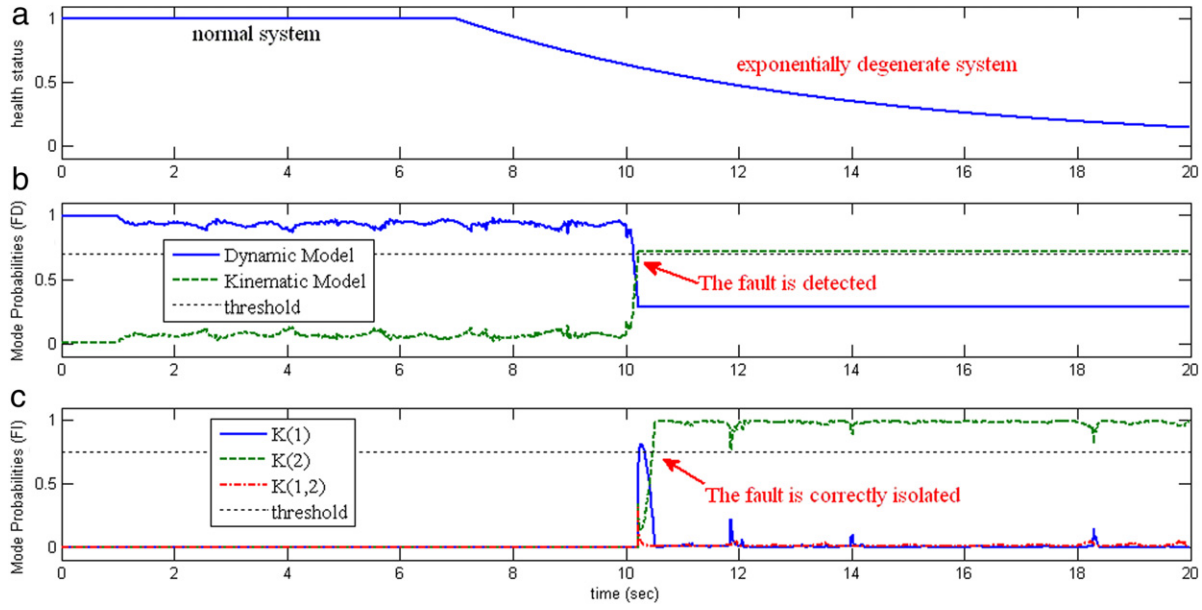

Fig. 12. (a) The "effective factor" of the 2nd joint. (b) Posterior mode probabilities of the dynamic model (solid line) and the kinematic model (dashed line). The fault is detected at $t = 10.21$ s. (c) Posterior mode probabilities of $K(1)$ (solid line), $K(2)$ (dashed line) and $K(1, 2)$ (dash–dot line). The faulty joint is isolated at $t = 10.51$ s.

Table 4
Summary of the experimental results.

Faults	Detection delay (s)	Isolation delay (s)
Type 1	0.04	0.08
Type 2	0.03	0.08
Type 3	0.03	0.08 (for the 1st fault) 0.11 (for the 2nd fault)
Type 4	0.07	0.37
Type 5	3.21	3.51

delay as acceptable since no significant performance deterioration was observed during this delay time.

The experimental results are summarized in Table 4. The detection delay and isolation delay refer to the time between the occurrence of the fault and the time at which the fault is detected and isolated, respectively. For the incipient fault (Type 5), the occurrence time of the fault refers to the time when the output torque starts decaying. It can be seen that all abrupt faults (Type 1–4) were detected and isolated successfully and immediately after their occurrences. Although the detection delay and the isolation delay for the incipient fault (Type 5) are longer, the tracking performance just deteriorates slightly when the fault is isolated. Therefore safe operation of the robot manipulator is still preserved.

6. Conclusion

In this paper, we proposed the HMM-FDI scheme as a solution to the model set design problem, which is the most challenging part of the conventional MM–FDI approaches. The HMM-FDI

scheme incorporated only a small number of models which are mixtures of the dynamic and kinematic equations of the robot manipulator. Therefore it is much more computationally efficient than conventional MM–FDI methods. In addition, the HMM-FDI scheme is applicable to various types of unexpected actuator faults, including abrupt faults, incipient faults, and simultaneous faults. Experiments were conducted on a two-joint robot manipulator. The experimental results verified the good performance of the HMM-FDI scheme.

References

[1] A.S. Willsky, A survey of design methods for failure detection in dynamic systems, Automatica 12 (1976) 601–611.
[2] P.M. Frank, Fault diagnosis in dynamic systems using analytical and knowledge-based redundancy—a survey and some new results, Automatica 26 (1990) 459–474.
[3] R. Isermann, Process fault detection based on modeling and estimation methods—a survey, Automatica 20 (1984).
[4] Q. Li, J.A. Bernard, Design and evaluation of an observer for nuclear reactor fault detection, IEEE Transactions on Nuclear Science 49 (2002) 1304–1308.
[5] H. Alwi, C. Edwards, Fault detection and fault-tolerant control of a civil aircraft using a sliding-mode-based scheme, IEEE Transactions on Control Systems Technology 16 (2008) 499–510.
[6] R. Isermann, R. Schwarz, S. Stolzl, Fault-tolerant drive-by-wire systems, IEEE Control Systems Magazine 22 (2002) 64–81.
[7] R. Rajamani, A.S. Howell, C. Chen, J.K. Hedrick, M. Tomizuka, A complete fault diagnostic system for automated vehicles operating in a platoon, IEEE Transactions on Control Systems Technology 9 (2001) 553–564.
[8] T. Hsiao, Detection and identification of sensor failures in vehicle lateral control systems, in: American Control Conference, New York, 2007, pp. 1636–1641.
[9] M.L. Visinsky, J.R. Cavallaro, I.D. Walker, Robotic fault detection and fault tolerance: a survey, Reliability Engineering & System Safety 46 (1994) 139–158.
[10] B.S. Dhillon, Robot Reliability and Safety, Springer-Verlag, 1991.
[11] H. Liu, G.M. Coghill, A model-based approach to robot fault diagnosis, Knowledge-Based Systems 18 (2005) 225–233.
[12] F. Caccavale, L. Villani, Fault diagnosis for industrial robots, in: Fault Diagnosis and Fault Tolerance for Mechatronic Systems: Recent Advances, Springer-Verlag, 2003.
[13] H. Schneider, P.M. Frank, Observer-based supervision and fault detection in robots using nonlinear and fuzzy logic residual evaluation, IEEE Transactions on Control Systems Technology 4 (1996) 274–282.
[14] D. Brambilla, L.M. Capisani, A. Ferrara, P. Pisu, Fault detection for robot manipulators via second-order sliding modes, IEEE Transactions on Industrial Electronics 55 (2008) 3954–3963.
[15] W.E. Dixon, I.D. Walker, D.M. Dawson, J.P. Hartranft, Fault detection for robot manipulators with parametric uncertainty: a prediction-error-based approach, IEEE Transactions on Robotics and Automation 16 (2000) 689–699.
[16] M.L. McIntyre, W.E. Dixon, D.M. Dawson, I.D. Walker, Fault identification for robot manipulators, IEEE Transactions on Robotics and Automation 21 (2005) 1028–1034.
[17] V. Verma, G. Gordon, R. Simmons, S. Thrun, Real-time fault diagnosis, IEEE Robotics & Automation Magazine 11 (2004) 56–66.
[18] V.F. Filaretov, M.K. Vukobratovic, A.N. Zhirabok, Parity relation approach to fault diagnosis in manipulation robots, Mechatornics 13 (2003) 141–152.
[19] B. Halder, N. Sarkar, Robust fault detection of a robotic manipulator, International Journal of Robotics Research 26 (2007) 273–285.
[20] A.T. Vemuri, M.M. Polycarpou, S.A. Diakourtis, Neural network based fault detection in robotic manipulators, IEEE Transactions on Robotics and Automation 14 (1998) 342–348.
[21] E.N. Skoundrianos, S.G. Tzafestas, Finding fault-fault diagnosis on the wheels of a mobile robot using local model neural networks, IEEE Robotics & Automation Magazine 11 (2004) 83–90.
[22] M. Nyberg, Model-based diagnosis of an automotive engine using several types of fault models, IEEE Transactions on Control Systems Technology 10 (2002) 679–689.
[23] Y. Zhang, X.R. Li, Detection and diagnosis of sensor and actuator failures using IMM estimator, IEEE Transactions on Aerospace and Electronic Systems 34 (1998) 1293–1313.
[24] N. Tudoroiu, K. Khorasani, Satellite fault diagnosis using a bank of interacting Kalman filters, IEEE Transactions on Aerospace and Electronic Systems 43 (2007) 1334–1350.
[25] S. Kim, J. Choi, Y. Kim, Fault detection and diagnosis of aircraft actuators using fuzzy-tuning IMM filter, IEEE Transactions on Aerospace and Electronic Systems 44 (2008) 940–952.
[26] J. Ru, X.R. Li, Variable-structure multiple-model approach to fault detection, identification, and estimation, IEEE Transactions on Control Systems Technology 16 (2008) 1029–1038.
[27] S. Suryanarayanan, M. Tomizuka, T. Suzuki, Design of simultaneously stabilizing controllers and its application to fault-tolerant lane-keeping controller design for automated vehicles, IEEE Transactions on Control Systems Technology 12 (2004) 329–339.
[28] J.T. Spooner, K.M. Passino, Fault-tolerant control for automated highway systems, IEEE Transactions on Vehicular Technology 46 (1997) 770–785.
[29] R.J. Patton, Fault-tolerant control systems: the 1997 situation, in: IFAC Symposium on Fault Detection Supervision and Safety for Technical Processes, 1997, pp. 1033–1055.
[30] J.D. English, A.A. Maciejewski, Fault tolerance for kinematically redundant manipulators: anticipating free-swinging joint failures, IEEE Transactions on Robotics and Automation 14 (1998) 566–575.
[31] A.A.G. Siqueira, M.H. Terra, C. Buosi, Fault-tolerant robot manipulators based on output-feedback H_{∞} controllers, Robotics and Autonomous Systems 55 (2007) 785–794.
[32] R.G. Robers, A.A. Maciejewski, A local measure of fault tolerance for kinematically redundant manipulators, IEEE Transactions on Robotics and Automation 12 (1996) 543–552.
[33] T.E. Menke, P.S. Maybeck, Sensor/actuator failure detection in the Vista F-16 by multiple model adaptive estimation, IEEE Transactions on Aerospace and Electronic Systems 31 (1995) 1218–1229.
[34] H.G. Sage, M.F.d. Mathelin, E. Ostertag, Robust control of robot manipulators: a survey, International Journal of Control 72 (1999) 1498–1522.
[35] S. Jeon, M. Tomizuka, T. Katou, Kinematic Kalman filter (KKF) for robot end-effector sensing, Journal of Dynamic Systems, Measurement, and Control 131 (2009) 021010.
[36] M.K. Kalandros, L. Trailovic, L.Y. Pao, Y. Bar-Shalom, Tutorial on multisensor management and fusion algorithms for target tracking, in: American Control Conference, Boston, Massachusetts, 2004, pp. 4734–4748.
[37] S. Thrun, W. Burgard, D. Fox, Probabilistic Robotics, The MIT Press, 2005.
[38] H.A. Aldridge, J.-N. Juang, Experimental robot position sensor fault tolerance using accelerometers and joint torque sensors, 1997.
[39] R. Kelly, V. Santibanez, A. Loria, Control of Robot Manipulators in Joint Space, Springer, 2005.
[40] T. Cacoullos, On upper and lower bounds for the variance of a function of a random variable, The Annals of Probability 10 (1982) 799–809.
[41] H.A.P. Blom, Y. Bar-Shalom, The interacting multiple model algorithm for systems with Markovian switching coefficients, IEEE Transactions on Automatic Control 33 (1998) 780–783.

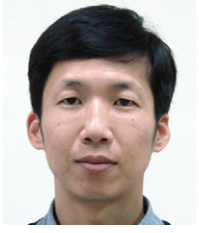

Tesheng Hsiao received his B.S. and M.S. degrees in control engineering from National Chiao Tung University, Taiwan, in 1995 and 1997 respectively, and the Ph.D. degree in mechanical engineering from the University of California, Berkeley, in 2005.

He is currently an assistant professor in the Department of Electrical Engineering at National Chiao Tung University, Taiwan. His research interests include advanced vehicle control systems, fault detection and isolation, and robotic motion control.

Mao-Chiao Weng received his B.S. degree in Mechanical Engineering from National Central University, Taiwan in 2006 and received his M.S. degree in Electrical Engineering from National Chiao Tung University, Taiwan in 2008.

He is currently with MediaTek Inc. His research interests include robotic motion control, and fault diagnosis of robot manipulators.